Simulations of a parallel plate Fission Chamber using the MCNPX simulation code

Ludovic Mathieu, Mourad Aiche

Simulations of a parallel plate Fission Chamber using the MCNPX simulation code

L. Mathieu[1,*], M. Aïche[1]

1) CENBG, CNRS/IN2P3-Université de Bordeaux, Chemin du Solarium B.P. 120, 33175 Gradignan, France

Abstract

MCNPX in its latest version is able to simulate the transportation of Fission Fragments. It opens the door to Fission Chamber simulations. Such simulations are not straightforward and comparisons with experimental spectra often failed. A procedure is described in the present paper to perform such simulation and to process the result to obtain realistic spectra. Simulated spectra are compared with experimental ones in various different conditions to validate the method and to present its limitations.

Keywords: parallel plate fission chamber, MCNPX simulations, alpha-FF discrimination

1. Introduction

Ionization chambers containing a deposit of fissile material (later on referred to as Fission Chambers - FC) are very simple and versatile devices [1] used in nuclear physics fundamental research, as well as in nuclear industry applications and nuclear energy research [2-4]. In the field of nuclear data measurements, FCs are typically used to tag fission events in coincidence or in anti-coincidence with other observables. This makes possible to study either fission-related quantities, such as fission cross-sections [5,6], prompt particle emission [7,8] or hardly observable phenomena, such as capture events [9]. FCs are also used as neutron flux monitors when the neutron-induced fission cross-section of the fissile deposit is very well known [10,11].

Fission events are identified by detecting at least one of the two Fission Fragments (FFs). These particles typically have to be discriminated from alpha particles arising from the natural radioactivity of the sample. The quality of this discrimination strongly depends on the characteristics of the FC itself and of the used deposit.

Typically Frish grids are implemented in FCs to obtain pulse-height signals independent of the ionization track position inside the detector. This is not the case in parallel plate FCs when, due to compactness requirements, the gap between the electrodes is few millimeters. In these FCs, the gap is much smaller than the range of the particles to be detected. In the projecting phase of these latter detectors, the design and optimization of the device rely on the capability of simulations to predict the pulse-height spectrum of incident particles, and in particular of alpha particles and fission fragments. Calculations are typically based on energy loss calculations [12], such as for instance SRIM/TRIM [6,8] or the PHITS code [13]. In few cases [14] simulations make use of the GEANT4 [15] package. However, to the best of our knowledge, the particle transport code MCNPX [16] has never been used

* Corresponding author, mathieu@cenbg.in2p3.fr, +33 5 57 12 08 04

for this purpose. Nevertheless, only a handful of previous works presents simulated "pulse-height spectra" rather than "energy deposition spectra" [8,12], and fewer can withstand the comparison with experimental data.

In this work, we present in Section 2 a simulation procedure to simulate the response to FFs and alpha particles of a parallel plate FC. In Section 3 and 4, simulated spectra for both a thin ^{252}Cf source and a thick ^{233}U fissile deposit respectively, are shown and compared to experimental data. The impact of different parameters (deposit characteristics, gap width, etc.) will be investigated and discussed in Section 5.

2. Method

The capability of the latest versions of MCNPX (2.6.0 and later) and of the more recent MCNP6 version to calculate the transport of heavy ions (i.e. nuclei heavier than helium) opened the possibility of using this code to simulate the detection of FF and alpha particles in fission chambers.

Our parallel plate FC consists of two plates of aluminum separated by a 5mm gap acting as cathode and anode. The volume is filled with a 90%Ar – 10%CH_4 gas mixture (referred to as P10 in the following) at a pressure of 1050 mbar.
A circular deposit is placed on the surface of the cathode. Its thickness is few hundreds of nanometers for the ^{233}U samples, and lower than a nanometer for the ^{252}Cf source. The deposits are assumed to be homogeneous and α-particles and FFs to be emitted isotropically from the deposit. The FF mass and energy distribution is given by the GEF code [17]. GEF is a semi-empirical model based on the observation of a common, general behavior of the fission properties of a broad variety of fissioning nuclei that is traced back to well-founded theoretical ideas. GEF calculates fission quantities with a precision that complies with the needs for applications in nuclear technology without specific adjustments to measured data of individual systems. The very good agreement of the predictions of GEF with evaluations or experimental data for the FF mass yields and FF kinetic energies of ^{252}Cf(SF) and ^{233}U(n_{th},f) and can be seen in figures 36, 127, 40 and 124 of [17], respectively.

A multi-steps procedure allows one to obtain the simulated pulse-height spectrum, to be compared to experimental data. First, the induced charge signal is calculated based on the particle energy deposition. Second, events where both the FFs deposit energy in the FC are accounted for. And finally the pile-up between different events is included. These steps are described in the following Sub-Sections.

2.1 Induced-charge signal calculation

Electrons are generated by the passage of a charged particle in the gas. They drift towards the anode inducing an electric signal. According to the Shockley-Ramo theorem [18,19], the pulse-height, I_c, of the induced signal, is proportional to the number of electrons (and hence to the deposited energy E_{dep}) and to the electron-drift distance x:

$I_c \alpha E_{dep} * x/d$

where d is the gap between the electrodes.
To convert the deposited energy into a pulse-height, the gap between electrodes is (virtually) divided into several parallel layers (typically more than 10). For a given particle ionization track, the energy

deposited in each layer, which corresponds to a given average x value, is retrieved from the MCNP PTRAC file and multiplied by the corresponding x/d ratio. The sum of the contributions of each layer gives the pulse-height for this track.

The deposited-energy (in black) and the pulse-height (in red) spectra produced by a ^{252}Cf source are shown in Figure 1, for α-particles (a) and FFs (b). Spectra are normalized to unit. The signal pulse-height is expressed in MeV, rather than in V as it should, to allow its direct comparison with the deposited energy. x/d values averaged on a given track range from 0.5 (particle track straight to the anode) to ~1 (particle track parallel to the cathode). This allows one to establish the relationship between the pulse-height and the particle-emission polar-angle. In the present experimental conditions, the FF ranges are between 1.5 cm and 3 cm depending on their initial kinetic energy. As the gap is only 5 mm, a FF can only deposit all its kinetic energy if it is emitted along the cathode. The FF heavy and light peaks are observed on the right part of the FF spectra, where x/d are close to one. The different parts of these spectra will be discussed thoroughly in Section 3.

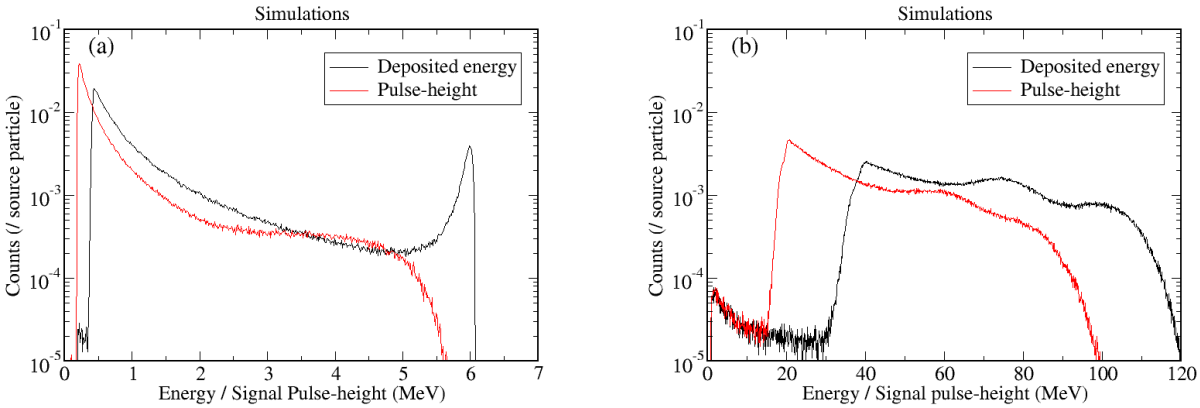

Figure 1: (Color online) Simulated deposited-energy spectra (black) and pulse-height spectra (red) for α-particles (a) and FFs (b) emitted from a ^{252}Cf source.

2.2 Simultaneous detection of the two fission fragments

In the fission process, two FFs are emitted back-to-back in the center-of-mass reference system, if we neglect eventual pre-scission neutron emission. Under certain conditions (no or negligible recoil of the fissioning nucleus) FFs are emitted back-to-back in the laboratory system. Usually, the FF emitted at backward angles ($\theta > 90°$ relative to the target normal) loses all its energy in the backing material of the deposit. However, if the FF is emitted at grazing angles ($\theta \sim 90\text{-}91°$), it may scatter in the backing and deposit some of its energy into the gas, inducing a signal. This signal adds to the signal of the FF emitted at the corresponding forward angle ($\theta = 89\text{-}90°$).

To implement this process in the final pulse-height spectrum, simulated FFs are divided into several $\cos(\theta)$ bins (with narrower bins for $\cos(\theta) \sim 0$) depending on the FF initial emission direction. A randomly chosen pulse-height from one $\cos(\theta)$ bin is added with a randomly chosen pulse-height of the $\cos(\theta+\pi)$ bin. It should be noted that this procedure does not take into account real FF couples. As there is nearly no dependence of the backward-emitted spectrum to the FF properties (mass and energy) such approximation can be made. Results from all $\cos(\theta)$ bins are then summed to obtain the final FF pulse-height spectrum.

Figure 2 shows the pulse-height spectrum when taking into account the “simultaneous detection of the two emitted FFs”, compared to the spectra obtained for the detection of only-forward (red, $\theta < 90°$) and only-backward (green, $\theta > 90°$) FFs. In the "only-backward" spectrum, events above and below 20 MeV correspond to events where FFs are emitted with $90° < \theta < 91°$ and $90° < \theta < 100°$, respectively. Indeed, the probabilities of a FF being scattered outside the backing are around 60% and 15%, for the two polar angle ranges, respectively. FFs emitted at angles greater than 100° have a very low probability to be scattered out of the backing, namely 0.5‰. The two-FFs spectrum obtained shows a high-energy tail, above the energy of the light-FF peak (above 100 MeV).

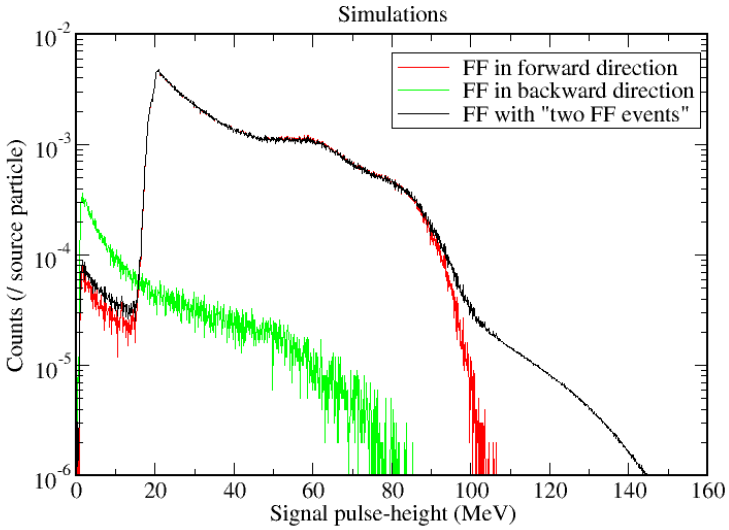

Figure 2: (color online) Simulated pulse-height spectra for FFs emitted in the only-forward (red) and only-backward (green) directions, and spectrum accounting for the “simultaneous detection of both FFs” (black).

2.3 Pile-up

Parallel plate ionization chambers are often used with highly α-active isotopes. In this case, the probability that the signal from an α-particles sums up in the ADC time window with the signal from a FF or another α-particle is not negligible. This effect has been taken into account for the correct simulation of pulse-height spectra, with the following procedure. One or several α-particle and/or FF events are randomly chosen accordingly to their activities and to the width of the time window. Gaussian or asymmetric triangular signals with given time constants are then randomly generated in the time window and summed. The maximum of the so-obtained signal gives the pulse-height of the event. Such procedure is obviously an approximation, since in reality the electronic signal processing is much more complex. In particular, for very high counting rates and/or slow electronic, baseline fluctuations due to non-ideal shape of signals can lead to a strongly reduced energy resolution. One to 100 billions events were simulated to properly account for low-probability events (high-multiplicity α pile-up, FF spectrum for highly radioactive sample, etc…).

Figure 3 shows α-particle (red) and FF spectra (green), normalized to their respective activities, as well as the α+FF spectrum, obtained accounting for the pile-up phenomenon. The pile-up effect mainly affects the high-energy tail of the α peak, around 10 MeV. One can notice the shape of the FF spectrum hidden under the α peak. This shape is in general agreement with the spectrum shown in [20] for the same ^{252}Cf source.

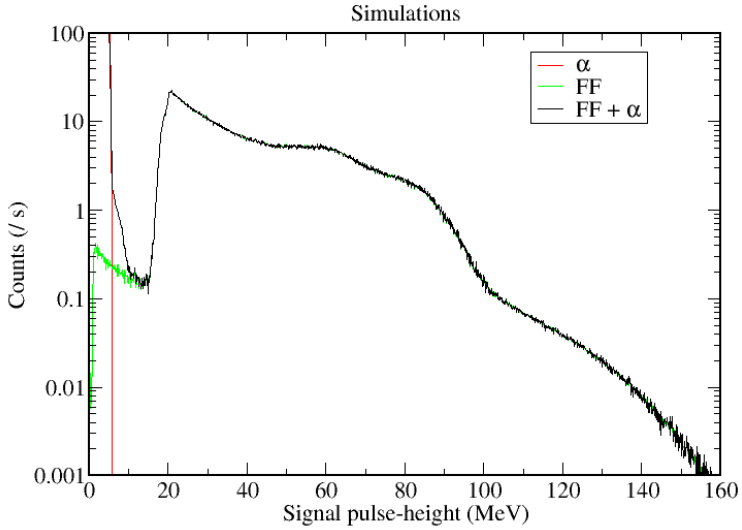

Figure 3: (color online) Simulated spectra for FFs (green) and α-particles (red) emitted by a 153kBq ^{252}Cf source, normalized by their activities (74 kBq in 2π for α emission and 4.7 kBq for spontaneous fission), and sum spectrum accounting for the pile-up effect (black) (gaussian signals, sigma: 0.1 µs, time window: 0.3 µs).

2.4 Energy resolution

As for other types of detectors, the same energy deposition along the same ionization track may lead to different pulse-height values, due to secondary electron production fluctuations, electron recombination fluctuations, electron screening effect, electronic noise, non-ideal electric field and gas contaminations. The energy resolution is often simulated as a Gaussian convolution with the spectrum, with a width that is function of the deposited energy. These parameters have to be measured experimentally.
Contrarily to gamma-ray or proton/alpha detectors, it is very difficult to experimentally measure the energy resolution of a parallel plate ionization chamber at FF typical energies. Indeed, FFs are not mono-energetic, and, given the small dimensions of the gap, part of their kinetic energy is deposited in the opposite electrode itself. Moreover, due to the absence of a Frisch-grid the pulse-height spectrum of mono-energetic particles is broad (it depends on the position of the ionizing track in the detector). For these reasons, in this work it is decided not to include energy resolution to the simulated results.

2.5 Post-processing procedure

The procedure described in Section 2 is summarized in Figure 4. Three different simulations are needed, and represented as gray rectangles. Analysis steps are shown in ellipses, while results are

presented in white rectangles. The impact of the different parameters in the simulation and in the pile-up procedure is schematized as rounded rectangles.

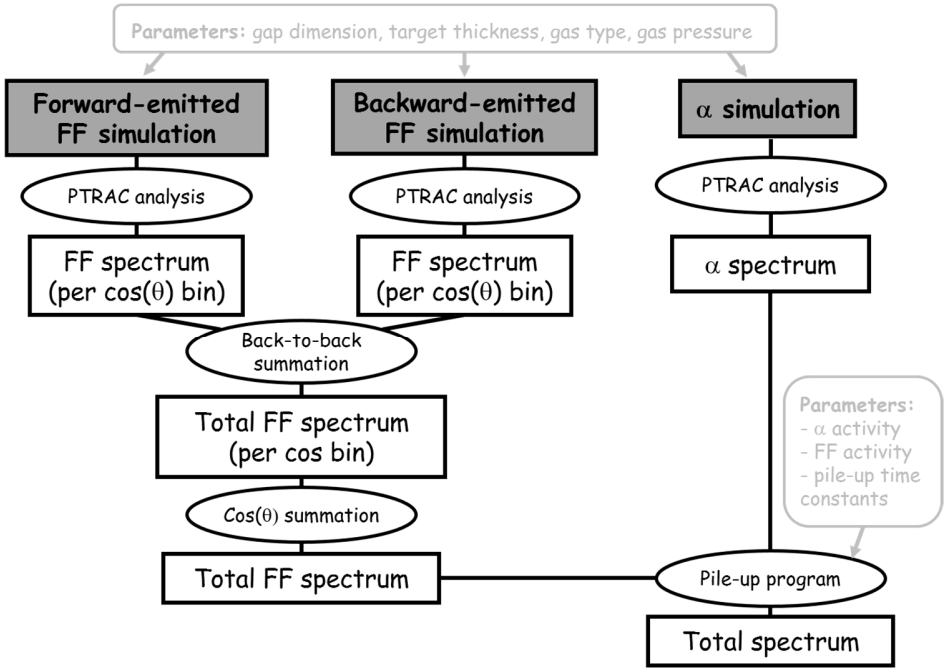

Figure 4: Steps of the simulation post-processing to infer the final FC spectrum including physics effects

3. Simulation of a ^{252}Cf source

3.1. Experimental spectrum

Measurements were carried out with a ^{252}Cf source placed in a parallel plate fission chamber. The aluminum electrodes were 12 cm in diameter separated by a 5.0 mm-wide gap. A 90%Ar – 10%CH_4 gas mixture at 1050 mbar was used. The bias voltage was 100 V, corresponding to the maximum electron mobility for the used gas (~5 cm/µs). The source, located at the center of the cathode, is constituted of a 5.04 mm-wide disk of 20 ng electrodeposited californium oxide on a nickel-clad platinum foil. The deposit was fixed by diffusion-bonding at 1000°C and is covered with a 50 µg/cm²-thick gold layer to prevent ^{252}Cf losses. The activity of the target was 153 kBq at the time of the measurements. The signal was collected on the anode via a CAMBERRA 2004 BT charge preamplifier. The experimental spectrum is shown in Figure 5a. In the insert, a spectrum with a lower threshold is presented to show the whole α peak.

Thanks to information provided by simulations, the different parts of the spectrum can be explained unambiguously, for the FFs as well as the α-particles:
- region a: lot of α particles emitted at low to medium polar angles, depositing only a small part of their kinetic energy in the gas,
- region b: few α particles emitted at high polar angles, depositing all their kinetic energy in the gas,
- region c: α particle pile-up with energies greater than the maximum α energy,

- region d: α-FF valley, populated by FFs emitted at grazing angles (see region i),
- region e: FFs emitted at very low polar angles and hitting the anode before having deposited all their kinetic energy into the gas. The two peaks corresponding to light and heavy FFs give rise to a shoulder in the simulated spectra (around 20 MeV), which is not visible in the experimental spectrum due to the poor energy resolution of the detector,
- region f: FFs emitted at high polar angles, depositing all their kinetic energy into the gas; heavy and light peaks can be seen,
- region g: FFs emitted at grazing angles, both simultaneously detected,
- region h: pile-up of FF signals from uncorrelated events
- region i: FFs emitted at grazing angles, losing part of their kinetic energy in the deposit itself. The residual energy deposited in the gas can be as low as zero.

The shape of the simulated pulse-height spectrum of alpha particles presented in Figure 1a is in very good agreement with the experimental result shown in the insert of Figure 5a. A quantitative comparison cannot be carried out, as the experimental spectrum cannot be calibrated. Indeed, the maximum alpha-particle energy is the only calibration point known with a good accuracy. This is because alpha particles emitted at high angle are stopped in the gas; therefore, the maximum deposited energy is nearly independent of the FC features.
On the contrary the light- and heavy-FF peaks are very broad, and their positions slightly depend on some unknown source features (as for instance the diffusion of sample atoms in the backing, see Section 3.2). Interestingly, the maximum of the FF spectrum (around channel 500) is quite narrow and independent of the source characteristic. But as FFs deposit only a part of their kinetic energy in the gas, the position of this peak depends on uncertain energy deposition calculation, which typically are affected by ~10% uncertainty. In addition, these calibration points are too close one to each other to obtain a reliable energy calibration. The maximum energy deposited by both FFs is more accurate and separated from the other points, but the determination of this calibration point suffers from strong experimental uncertainties.

3.2. Simulated spectrum

Following the steps detailed in Section 2, a simulated spectrum was calculated and it is shown as a black line on Figure 5b. Although there is a rather good global agreement between the simulated and experimental spectra, a strong discrepancy can be observed in the height of the FF peaks, which appear more prominent in the simulated spectrum.
An additional step must be taken into account when dealing with very thin deposits, as the ^{252}Cf sources. Indeed, the average thickness of the californium deposit is lower than one atomic layer while that of the gold layer is 26 nm. These dimensions must be compared to the roughness of the backing. In addition, the 1000°C thermal treatment of the Cf deposit could have induced the diffusion of californium atoms into the backing. To characterize and simulate these effects is beyond the scope of this work. It was therefore assumed that ^{252}Cf nuclei are uniformly distributed over a given depth in the backing. Different geometrically increasing implantation depths have been tested. The spectra for a maximum implantation depth of 30, 100 and 300 nm are shown in Figure 5b. For higher implantation depths, the FF peaks are less pronounced and the slope of the “both FFs events” tail increases. This effect clearly reduces the discrepancies when compared to the experimental spectrum, although the agreement is not perfect. Other implantation profiles (for instance more ^{252}Cf atoms near the surface) have been simulated and lead to the same conclusion. The remaining discrepancy can be attributed to

the non-ideal experimental device (homogeneity of the gold layer, electrodes parallelism...) compared to the simulated system. In the following, the presented simulations assume a maximum implantation depth of 30 nm with a uniform distribution.

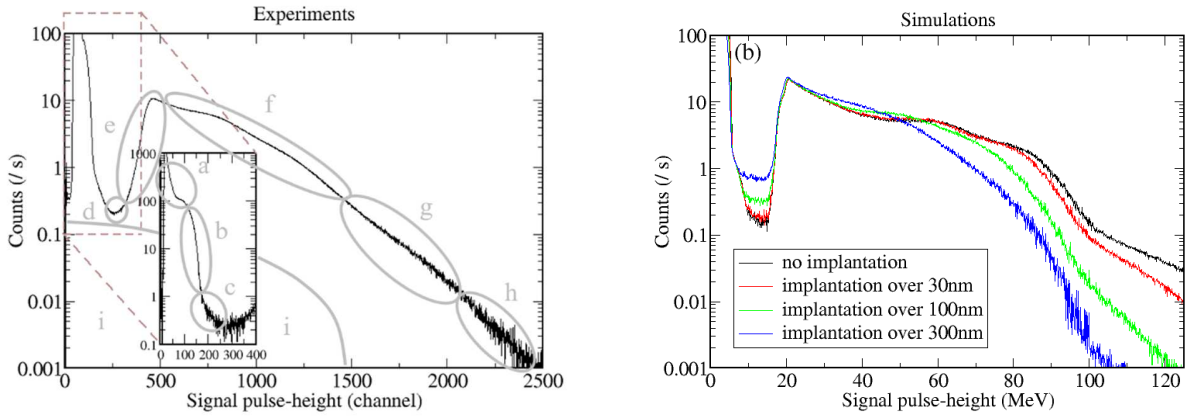

Figure 5: (Color online) (a) Experimental spectrum of a ^{252}Cf source. The insert shows the α contribution obtained in a dedicated measurement with a lower threshold; (b) Simulated spectra of a ^{252}Cf source obtained assuming different maximum implantation depths into the backing: 0, 30, 100 and 300 nm (see text).

The aim of FC simulations can be to infer the FF detection efficiency. This parameter and its accuracy are crucial for some experiments using FCs [8,9,20,21]. The depth and the width of the α-FF valley are key parameters to determine the FC efficiency. Indeed, an experimental threshold is usually set in the α-FF valley and FFs below this threshold are treated as not-detected.
The simulated efficiency significantly depends on experimental parameters, like the implantation depth, which are typically not known and introduce a large uncertainty. For instance, assuming a α-FF threshold at 10 MeV in the pulse-height spectrum, the obtained detection efficiencies are of 99.1%, 98.0%, 97.1% and 94.2% for implantation depths of 0, 30, 100 and 300 nm, respectively. These values have to be compared to the uncertainty associated to the experimental efficiency, measured via the prompt fission neutrons method [20], which is of (98.7±0.2)%. Therefore, it turns out that simulations cannot be used to obtain an accurate value of fission detection efficiency.

4. Simulation of a thick ^{233}U target

The procedure described in Section 2 was applied to thick targets. A ^{233}U target (U_3O_8 chemical form) produced by EC-JRC-Geel, with a thickness of about 250 µg/cm² and a diameter of 6 cm, was considered. The α-activity was 2.5 MBq. The irradiation of the target with a thermalized neutron flux at the AIFIRA facility is presented in Ref. [22]. The fission rate was about 40 fission/s, which is a very low rate when compared to the one of the described ^{252}Cf source. The signal was treated with an analogic electronics and a shaping time of 0.25 µs.

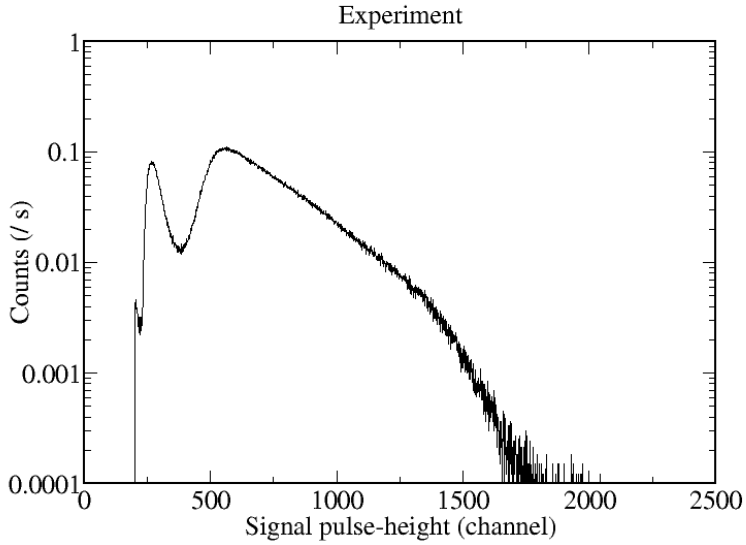

Figure 6: Experimental pulse-height spectrum for a 250 µg/cm² ^{233}U target in thermal neutron flux.

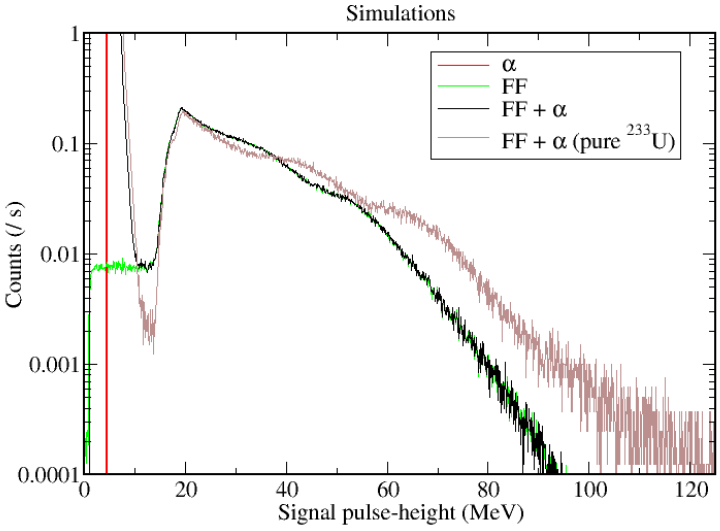

Figure 7: (color online) Simulated pulse-height spectra for a 250 µg/cm² ^{233}U target (296 µg/cm² of U_3O_8) as well as for a chemically pure ^{233}U target.

The experimental and the simulated spectra are shown in Figure 6 and Figure 7, respectively. The impact of the target thickness is important on the FF high-energy tail, which drops quickly. Structures can be seen in the simulated spectrum, but not in the experimental one. On the contrary, the sample thickness has little impact on the "low polar angle" FF peak at about 20 MeV. Indeed, a typical ^{233}U FF (^{89}Kr with a kinetic energy of 107 MeV) emitted in the forward direction deposits 0 to 3.5 MeV in

the target, depending on the depth of the emission point, whereas the energy deposition in the gas only ranges from 24.7 MeV (for a surface emission) to 24.4 MeV (for a 250 µg/cm²-deep emission).

Given the high α counting rate, the α-FF valley is partly filled with α pile-up. Indeed, in the experimental spectrum as well as the simulated one, a smaller slope of the α tail can be observed when compared to the one of the ^{252}Cf source (see Figure 5).
Moreover, the simulated FF spectrum below the α pic is rather flat, contrary to what was found for the ^{252}Cf case. This support the efficiency determination technique consisting in extrapolating to zero signal amplitude the floor of the α-FF valley, while it reject the assumption of a linear decrease of the FF yield down to 0 for zero energy deposition [12].

In Figure 7 the spectra obtained for a chemical pure and for the oxide U target are compared. The observed differences in the spectra arise from the presence of light but numerous oxygen atoms that participate to the particle energy loss in the target. It should be noted that the sensitivity of the spectrum to the target composition introduce an additional issue in the pulse-height spectrum simulation, as the real chemical composition of the target is not completely known. Indeed, other impurities (like O, C, N or F) may be present in the target in high quantity [23]. The target chemical composition also influences the simulated FF detection efficiency. For instance, setting a threshold in the α-FF valley, the simulated efficiencies are 94.2 and 96.9% for U_3O_8 and the pure ^{233}U sample, respectively.

5. Sensitivity analysis

5.1. Influence of the signal treatment

As mentioned in Section 2.3, the electronics signal treatment has an influence on the results of the pile-up effect. Combinations of FF- and α-simulated spectra for the ^{252}Cf source applying different electronic treatments (width of signals) have been carried out and are shown in Figure 8a. The different treatments can be schematically separated in fast and slow treatments, where the former are characterized by the use of shaping times of the order of 0.25 µs while the latter by shaping times of the order of 1 µs. A slow treatment of signals implies the presence of more events in the same time window, leading to an increase of α pile-up. This effect is observed both on the simulated and the experimental spectra (Figure 8b), as an increase of events on the right side of the alpha peak. A similar behavior is observed when the activity increases (more alphas in the same time window), as shown in Figure 9. This indicates the importance of using fast electronics, especially when the activity of the target is high (typically above 1 MBq). The high-energy part of the FF spectra, not shown in these figures, is not affected by the pile-up effect, even for high α-activities.

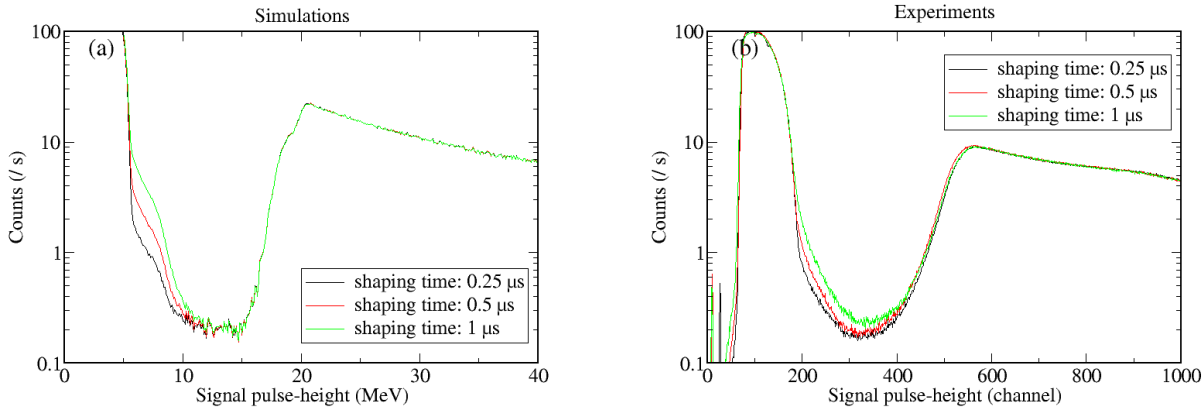

Figure 8: (Color online) Simulated (a) and experimental (b) ^{252}Cf spectra obtained using three different shaping times, namely 0.25µs (black), 0.5µs (red) and 1µs (green).

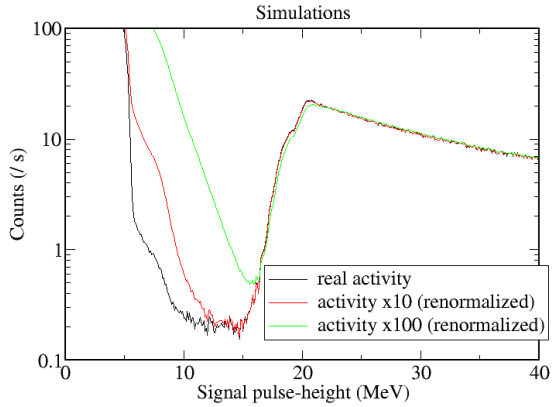

Figure 9: (Color online) Simulated spectra of a ^{252}Cf source with three different activities, namely 153kBq (black), 1530kBq (red) and 15 300kBq (green).

5.2 Influence of the bias

In typical PP FC, the sample to be studied is deposited on the cathode and electrons generated in the gas drift to the opposite electrode (anode). This implies that, closer the ionization track is to the cathode stronger is the induced signal. The opposite is true when reversing the FC polarity [12]: electrons produced by tracks close to the deposit (now the anode) will induce a weak signal. Simulated spectra with normal and reversed bias are shown in Figure 10a, while experimental spectra are shown in Figure 10b. It can be seen in both figures how reversed bias induce a less deep α-FF valley, which is filled with FF emitted at high polar angle. When the fissile material is deposited on both electrodes ("double-side coating" [24]), the FC spectrum is the sum of both spectra (grey line in Figure 10a).

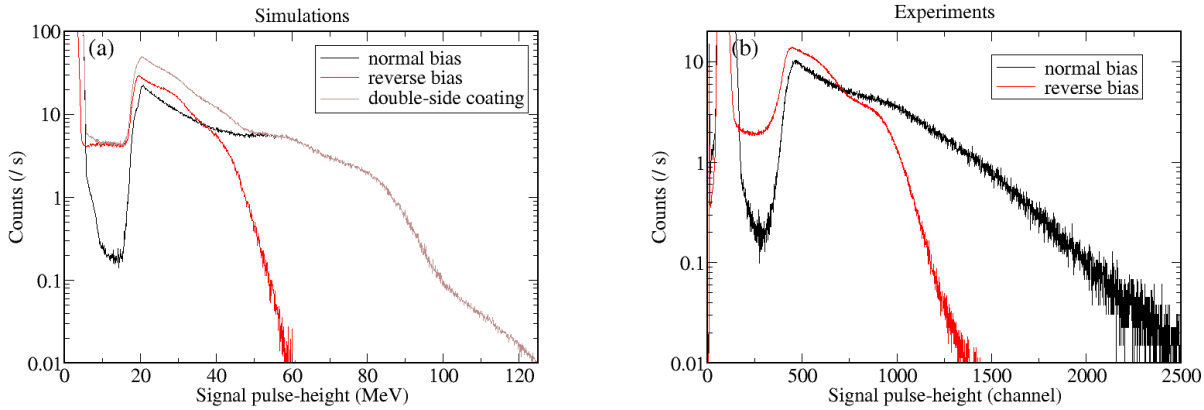

346 **Figure 10:** (Color online) Simulated (a) and experimental (b) ^{252}Cf spectra obtained applying normal
347 (black) or reversed (red) bias.

348
349 **5.3 Influence of the gas thickness**
350
351 The pulse-height signal generated by a FC strongly depends on the amount of matter presents between
352 the electrodes, as it determines the energy deposited by α-particles and FFs. Both the gas pressure and
353 the gap dimension determine the "gas thickness", with roughly the same impact, provided that
354 particles do not escape the active volume of the FC. Figure 11 shows the effect of the gas thickness
355 (via a modification of the gap dimension) on the simulated and experimental FC spectra.

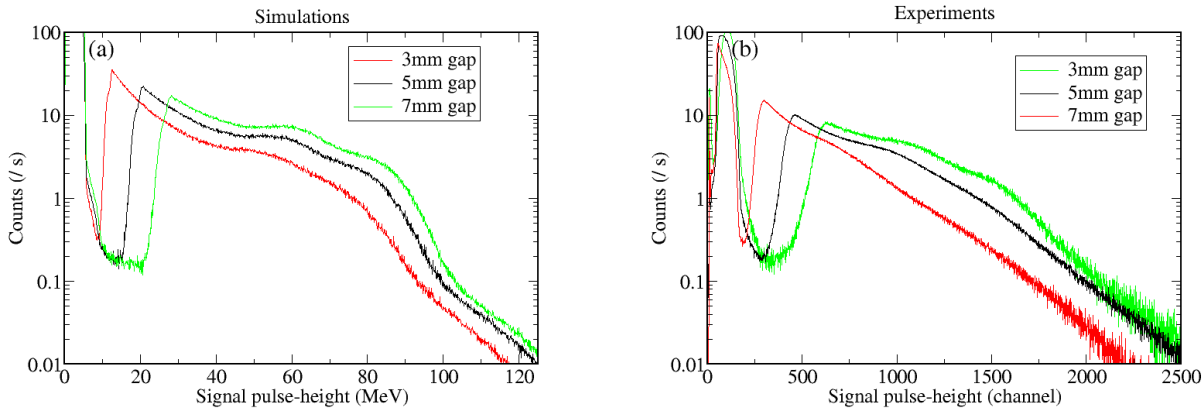

356 **Figure 11:** (Color online) Simulated (a) and experimental (b) ^{252}Cf spectra for three different gas
357 thicknesses, namely 3mm (red), 5mm (black) and 7mm (green).

358 A bigger gas thickness increases the energy deposited by α or FF before hitting the opposite electrode
359 (i.e. emission at low polar angles), but has little influence on particles depositing all their energy in the
360 gas (i.e. emission at high polar angles). As discussed in Section 3.2, the left side of the α-FF valley is
361 determined α-particles depositing all their kinetic energy, while the right side by FFs depositing a
362 small part of their kinetic energy. Therefore, a bigger gas thickness leads to a wider α-FF valley and

thus to a better α-FF discrimination. The bottom of the α-FF valley is determined by FFs emitted at grazing angle and, therefore, it is not affected by the gas thickness.
MCNPX simulations use tabulated stopping powers, which are poorly known quantities [25]. Adjustments are sometimes made on simulated spectra [8] to fit the experimental data. An error in stopping powers of FFs in the gas would be similar to a change in the gas thickness.

5.4. Influence of target thickness

The sample thickness is one of the main concerns when optimizing the design of a FC. Thicker targets give better statistics at the cost of an increased energy loss of FF and therefore a lower α-FF discrimination. No experimental data are available to validate the simulations, so these are variants of the ^{233}U simulation presented in Section 4. Figure 12a presents the simulated spectra obtained for different thicknesses of ^{233}U (U_3O_8 chemical form), namely 125, 250, 500 and 1000 µg/cm2.
As discussed in Section 4, the sample thickness primarily affects the high-energy tail of the FF spectrum and the α-FF valley, since both regions are populated by FFs emitted at high or grazing angles. Structures in the FF spectrum also disappear as the sample thickness increases. The first FF peak around 20 MeV is only slightly affected, because FFs emitted at low angles do not lose a significant part of their kinetic energy in the target, independently of its thickness. The fission detection efficiencies are 96.8, 94.2, 88.0 and 76.3%, for thicknesses of 125, 250, 500 and 1000 µg/cm², respectively. The main part of undetected FFs stop in the deposit, with a non-exiting proportion of 3.0%, 4.5%, 8.2% and 17.0%, respectively.

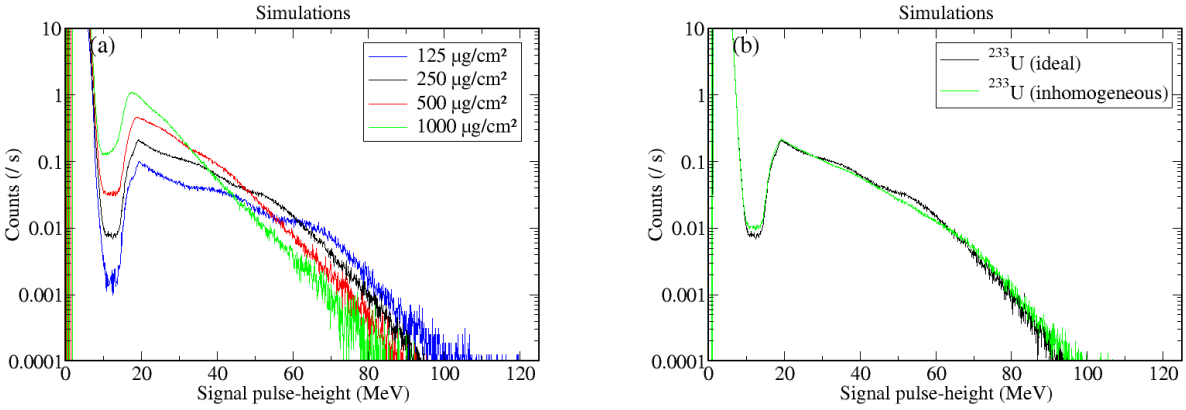

Figure 12: (Color online) Simulated spectra of ^{233}U targets (U_3O_8 form) (a) with different homogeneous thicknesses of ^{233}U, namely 125, 250, 500 and 1000 µg/cm²; (b) with homogeneous (black) or inhomogeneous (green) thicknesses.

Real samples are often inhomogeneous. Spectra arising from thinner and thicker parts of the target mix up. This leads to a mixed high-energy tail, making FF structures to disappear meanwhile the first FF peak remains quite unchanged. The behavior of an inhomogeneous sample was calculated by averaging the spectra for different thicknesses (125, 250 and 500 µg/cm² with weights of 2, 1 and 0.5 respectively, resulting in an averaged thickness of 250 µg/cm²). The result is presented in Figure 12b. The obtained spectrum seems in very good agreement with the experimental data presented in Figure 6, especially for the absence of structures and for the slope change in the FF part of the spectrum.

5.5 Influence of the gas type

Several gases are suitable to be used in FC, and P10 is one of the most common. CF_4 is also often used, for its very high electron mobility. Moreover, this gas has a molar mass of 88 g/mol to be compared to 37.6 g/mol of P10. This induces a very large α-FF valley due to the increased gas thickness. This effect can be clearly seen on the simulated spectra presented in Figure 13a. On the contrary, the two FF peaks are approximately at the same position.
Figure 13b presents comparable experimental spectra (using different bias to obtain the same electron drift velocity), which are in clear disagreement with simulations. When using CF_4, the valley is partly filled with FFs (αs are more or less unaffected), and FF peaks as well as high-energy tail are shifted to lower energies. It should be kept in mind that similar experimental spectra have been previously reported in literature [24,26], although an efficient signal treatment allows for some improvements [27].

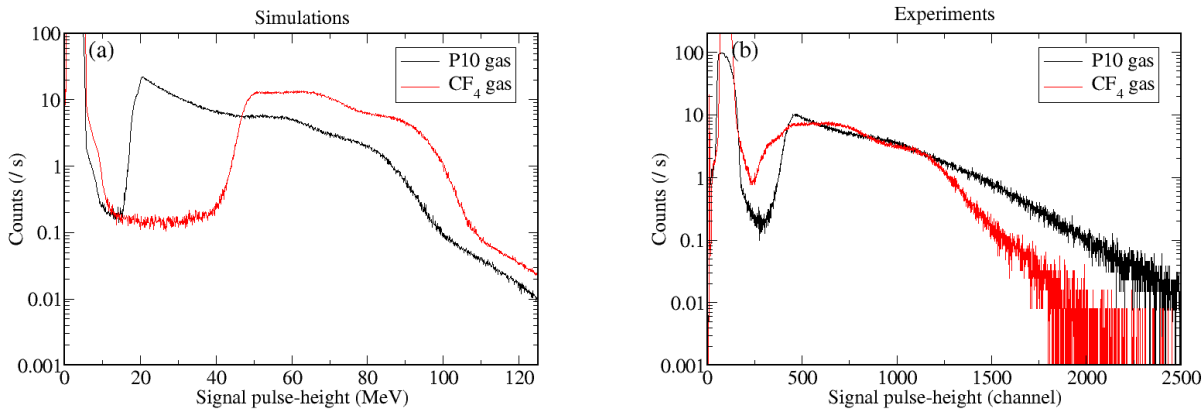

Figure 13: (Color online) Simulated (a) and experimental (b) ^{252}Cf spectra obtained using P10 (black) and CF_4 (red) gases at about the same electron drift velocities.

Usually, the broad shape of the FF spectrum is attributed to the target thickness, however, as previously shown, it has nearly no influence on the position and narrowness of the first FF peak. The present experiment was carried out using the same ^{252}Cf source and changing the type of gas in the FC. It therefore proves the broad spectrum observed using the CF_4 gas arise from the use of the gas itself. Several tests were carried out with different electron drift velocities with CF_4 gas, as well as with P10 gas. It was observed that different shapes of the FC spectrum could be attributes to different gas mobilities. The electron drift velocity is not taken into account in our simulations. Moreover, spectra presented in literature obtained using different gases (90%Xe-10%CF_4 [15], isobutene [28], methane [29]) show a behavior similar to the P10 gas spectrum. The unexpected shape of the spectrum obtained using CF_4 gas is certainly related to the electron drift in the gas [30], therefore additional studies of CF_4 properties would be required to obtain better simulated spectra.

6. Conclusion

Simulations have been carried out with MCNPX, and a post-processing procedure has been developed to reproduce parallel plate Fission Chamber spectra. The overall agreement between experimental and simulated spectra is rather good, as the global features of experimental spectra are reproduced. This

provides unambiguous explanations on the physical processes involved, as the relationship between the spectrum shape and the particle emission polar angle, the energy lost in the target and the simultaneous detection of both the emitted FFs. The procedure has been used by the n_ToF collaboration with MCNPX and GEANT4 simulations [26].
Nevertheless, the accuracy of the simulations is limited by the knowledge of the experimental conditions (especially the source/target characteristics). In particular, these simulations cannot be used to infer the fission detection efficiency with a good accuracy. Moreover, they fail to reproduce spectra using CF_4 gas, due to specific electronic drift phenomena not implemented here. Multi-physics simulations, including FF-energy loss, electron production and drift in a specific gas may lead to more detailed and accurate results.

References

1. G. F. Knoll, Radiation Detection and Measurement, 4th Edition, Wiley, 2011
2. IAEA, https://ansn.iaea.org (accessed on October 1st, 2018)
3. B. Geslot et al., Development and Manufacturing of Special Fission Chambers for In-core Measurement Requirements in Nuclear Reactors, Proc. ANIMMA, Marseille, France, 2009
4. Y. Jinwei et al., Development of Prototype Neutron Flux Monitor for ITER, Plasma Sci. and Tech., 7, No. 3 (2005) p. 2860
5. S. A. Wender et al., A fission ionization detector for neutron flux measurements at a spallation source, Nucl. Instr. and Meth. A, **336** (1993) p. 226
6. M. Calviani et al., A fast ionization chamber for fission cross-section measurements at n_TOF, Nucl. Instr. and Meth. A, **594** (2008) pp. 220-227
7. R. Billnert et al., New prompt spectral γ-ray data from the reaction ^{252}Cf(sf) and its implication on present evaluated nuclear data files, Phys. Rev. C **87**, 024601 (2013)
8. A. Chatillon et al., Measurement of prompt neutron spectra from the 239Pu(n,f) fission reaction for incident neutron energies from 1 to 200 MeV, Phys. Rev. C **89**, 014611 (2014)
9. I. Companis et al., Measurement of neutron capture and fission cross sections of ^{233}U in the resonance region, Proc. CNR*11, Prague, Czech Republic, 2011
10. P. Filliatre et al., Reasons why Plutonium 242 is the best fission chamber deposit to monitor the fast component of a high neutron flux, Nucl. Instr. and Meth. A, **593** (2008), pp. 510-518
11. R. Nolte and D. J. Thomas, Monoenergetic fast neutron reference fields: II. Field characterization, Metrologia **48** (2011), pp. 274-291
12. A. Plompen et al., Method Developing and Testing for Inelastic Scattering Measurements at the GELINA Facility, Journ. of Kor. Soc., Vol. **59**, No. 2, 1581 (2011) pp. 1581-1584
13. M. Nakhostin et al., A Fast Response and γ-insensitive Neutron Detector based on Parallel-Plate Avalanche Counter, Rad. Prot. Dos., Vol. **129**, No. 4 (2007) pp. 426-430
14. T. Kögler et al., Fission Experiments at nELBE, Phys. Proc., **47** (2013) pp. 178-183
15. S. Agostinelli et al., Geant4—a simulation toolkit, Nucl. Instrum. Meth. A, **506** (2003) pp. 250-303
16. D. B. Pelowitz et al., MCNPX 2.7.C Extensions, LANL Report No. LA-UR-10-00481 (2010)
17. K.-H. Schmidt et al., General Description of Fission Observables: GEF Model Code, Nucl. Data Sheets **131** (2016) pp. 107-221
18. W. Shockley et al., Currents to Conductors Induced by a Moving Point Charge, J. Appl. Phys., **9**, 635 (1938)
19. S. Ramo et al., Currents Induced by Electron Motion, IRE Proc., **27**, 584 (1939)

20. L. Mathieu et al., Accurate measurement of a fission chamber efficiency using the prompt fission neutron method, Proc. International Conference on Nuclear Data for Science and Technology, 03016, Bruges, Belgium, 2016, EPJ Web of Conference
21. P. Marini et al., Prompt Fission Neutrons in the ^{239}Pu(n,f) Reaction, arXiv:1902.07951
22. I. Companis, Univeristy of Bordeaux PhD thesis, *in French* (2013)
23. G. Sibbens et al., Proc. 28th World Conference of the International Nuclear Target Development Society, Cape Town, South Africa, 2016
24. J. Taieb et al., A new fission chamber dedicated to Prompt Fission Neutron Spectra measurements, Nucl. Instr. and Meth. A, **833** (2016) pp. 1-7
25. P. Filliatre et al., Stopping power of fission fragments of ^{252}Cf in argon: A comparison between experiments and simulation with the SRIM code, Nucl. Instr. and Meth. A, **618** (2010) pp. 294-297
26. M. Bacak et al., A compact multi-plate fission chamber for the simultaneous measurement of 233U capture and fission cross-sections Proc. International Conference on Nuclear Data for Science and Technology, 03027, Bruges, Belgium, 2016
27. J. Taieb, *private communication*
28. K. Hirose et al., Multi-layered parallel plate ionization chamber for cross-section measurements of minor actinides, Nucl. Instr. and Meth. A, **621** (2010) pp. 379-382
29. E. Blain et al., A method to measure prompt fission neutron spectrum using gamma multiplicity tagging, Nucl. Instr. and Meth. A, **805** (2016) pp. 95-100
30. L.G. Christophorou et al., Electron Interactions with CF_4, J. Phys. Chem. Ref. Data, Vol. **25**, No. 5 (1996)